

# Analysis of Laminar Forced Convection Condensation Within Thin Porous Coatings

K. J. Renken,\* M. J. Carneiro,† and K. Meechan†  
University of Wisconsin—Milwaukee, Milwaukee, Wisconsin 53201

The effect of laminar forced convection on enhanced filmwise condensation within thin inclined porous coatings is numerically investigated. The model simulates two-dimensional condensation within very permeable and highly conductive porous substrates. The Darcy-Brinkman-Forchheimer model is utilized to describe the flowfield within the porous layer while classical boundary-layer equations are employed in the pure condensate region. The numerical results document the dependence of the temperature field and the heat transfer rate on the governing parameters such as the Reynolds number, the Rayleigh number, the Darcy number, the Jakob number, the Prandtl number, as well as the porous coating thickness and effective thermal conductivity. The results of this study provide valuable fundamental predictions of enhanced film condensation that can be used in a number of practical thermal engineering applications.

## Nomenclature

$c_p$	= specific heat, J/kg-K
$Da$	= Darcy number
$F$	= flow inertia term
$g$	= gravitational acceleration, m/s <sup>2</sup>
$H$	= thickness of porous coating, m
$h$	= convective heat transfer coefficient, W/m <sup>2</sup> -K
$h_{fg}$	= heat of evaporation, J/kg
$Ja$	= Jakob number
$K$	= permeability, l/m <sup>2</sup>
$k$	= thermal conductivity, W/m-K
$L$	= length of surface, m
$Nu_x$	= local Nusselt number
$P$	= pressure, N/m <sup>2</sup>
$Pe$	= Peclet number
$Pr$	= Prandtl number
$q''$	= heat flux, W/m <sup>2</sup>
$Ra$	= Rayleigh number
$Re$	= Reynolds number
$T$	= temperature, K
$U_\infty$	= freestream vapor velocity, m/s
$u$	= x-component velocity, m/s
$v$	= y-component velocity, m/s
$w$	= mass flow rate of condensate per unit depth, kg/s-m <sup>2</sup>
$x$	= vertical coordinate, m
$y$	= horizontal coordinate, m
$\alpha$	= thermal diffusivity, m <sup>2</sup> /s
$\beta$	= coefficient of thermal expansion, 1/K
$\delta$	= film condensation thickness, m
$\varepsilon$	= porosity
$\theta$	= dimensionless temperature
$\lambda$	= inertia parameter
$\mu$	= dynamic viscosity, kg/m-s
$\nu$	= kinematic viscosity, m <sup>2</sup> /s
$\rho$	= density, kg/m <sup>3</sup>

## Subscripts

$e$	= effective
$f$	= fluid

$l$	= liquid
$ref$	= reference
$sat$	= saturation
$v$	= vapor
$w$	= condensing surface
$\infty$	= freestream
$'$	= modified

## Superscript

*	= dimensionless
---	-----------------

## Introduction

THE problem of condensation heat transfer has been given extensive attention since the pioneering work of Nusselt.<sup>1</sup> Recently, the problem of condensation promotion within a porous medium has become an important subject because of its application in heat pipe technology, underground nuclear waste repositories, geothermal reservoirs, building insulation materials, spacecraft condensers, and packed bed reactors.

Past investigations on condensation in a porous region that are relevant to the present include the founding works of Cheng<sup>2</sup> and Cheng and Chiu,<sup>3</sup> who studied the problem of steady and transient film condensation along an inclined surface embedded in a porous medium filled with dry saturated vapor. Solutions were obtained for the temperature and flowfields based on the assumption of a distinct boundary layer between the condensate and the vapor (albeit, no two-phase zone in between). Udell<sup>4,5</sup> developed a one-dimensional, steady-state model of heat transfer in porous media (heat pipes) with the inclusion of the effects of capillarity, gravity forces, and phase change. Poulikakos and Orozco<sup>6</sup> reported a theoretical study of film condensation outside a vertical pipe containing a cold fluid and embedded in a porous medium. Kaviani<sup>7</sup> provided boundary-layer and similarity solutions of film condensation within a porous matrix, while White and Tien<sup>8,9</sup> presented experimental and analytical results.

Plumb<sup>10</sup> demonstrated that capillary effects and the introduction of a two-phase region play significant roles during film condensation in porous media. Later, Shekarraz and Plumb<sup>11,12</sup> used a one-dimensional model and experimental measurements to investigate the influence of capillary porous fins on filmwise condensation. Majumdar and Tien<sup>13</sup> using phase equilibrium thermodynamics verified the Plumb<sup>10</sup> model of a two-phase zone during porous media film condensation. Plumb et al.<sup>14</sup> and Chung et al.<sup>15</sup> have also provided experimental and numerical data of condensation on a cold vertical surface submerged in a packed bed of glass beads.

Received May 10, 1993; revision received Sept. 8, 1993; accepted for publication Sept. 9, 1993. Copyright © 1993 by the American Institute of Aeronautics and Astronautics, Inc. All rights reserved.

\*Associate Professor, Department of Mechanical Engineering, P.O. Box 784. Member AIAA.

†Graduate Research Assistant, Department of Mechanical Engineering.

More recently, Renken et al.<sup>16</sup> introduced a viable alternative technique for heat transfer enhancement during film condensation that employs a relatively thin, very permeable, and highly conductive porous coating which is attached to a condensing surface. Further analysis<sup>17</sup> and experimentation<sup>18,19</sup> of this condensation enhancement method have shown significant increases in the heat transfer coefficient as compared to the classical plain surface case.

This article presents an extension of the previous works by supplying a numerical study of laminar forced convection condensation over a porous/fluid composite system. The composite system is composed of a freestream flow of pure saturated vapor overlaying a thin porous substrate which is affixed to a cold inclined flat plate. This fundamental investigation is aimed at the interacting phenomena occurring in the condensate-saturated porous substrate. The effects of the various governing parameters on the heat transfer and fluid flow of the problem are analyzed.

### Analysis

#### Mathematical Formulation

A schematic of the physical model and its coordinate system are shown in Fig. 1. The thickness of the porous substrate is  $H$ , the freestream vapor velocity is  $U_\infty$ , and the temperature of the flowing vapor is  $T_\infty$ , which is equivalent to the saturation temperature of the vapor. The cold vertical surface is isothermal and at temperature  $T_w$  ( $T_w < T_\infty$ ). In the present analysis, the flow is assumed steady, laminar, two-dimensional, and incompressible. In addition, the thermophysical properties of the fluid and the porous coating are assumed to be constant and the fluid-saturated porous substrate is considered homogeneous and isotropic. The condensate and the vapor regions are separated by a distinct boundary, with no two-phase zone in between. By making this assumption, the complexity of dealing with a two-phase region and the relative permeability no longer exists.

The mathematical model of the problem is described by two subregions, each of which has its own set of governing equations. In the pure fluid region, the conservation of mass, momentum, and energy are

$$\frac{\partial u}{\partial x} + \frac{\partial v}{\partial y} = 0 \quad (1)$$

$$u \frac{\partial u}{\partial x} + v \frac{\partial u}{\partial y} = \frac{g(\rho_f - \rho_v)}{\rho_f} + \nu_f \frac{\partial^2 u}{\partial y^2} \quad (2)$$

$$u \frac{\partial T}{\partial x} + v \frac{\partial T}{\partial y} = \frac{k_f}{\rho_f c_p} \frac{\partial^2 T}{\partial y^2} \quad (3)$$

The conservation equations for the porous substrate zone are based on the Darcy-Brinkman-Forchheimer (D-B-F) model which includes the effects of flow inertia as well as friction caused by macroscopic shear. The D-B-F model was chosen so that the generality of the problem formulation remained. The governing equations for this subregion are

$$\frac{\partial u}{\partial x} + \frac{\partial v}{\partial y} = 0 \quad (4)$$

$$u \frac{\partial u}{\partial x} + v \frac{\partial u}{\partial y} = \frac{-\nu_e}{K} u - \frac{F\varepsilon}{K^{1/2}} u^2 + \nu_e \frac{\partial^2 u}{\partial y^2} + \frac{g(\rho_f - \rho_v)}{\rho_f} \quad (5)$$

$$u \frac{\partial T}{\partial x} + v \frac{\partial T}{\partial y} = \frac{k_e}{\rho_f c_p} \frac{\partial^2 T}{\partial y^2} \quad (6)$$

where, Eqs. (2) and (5) have utilized the conditions

$$y \rightarrow \infty: \quad u = U_\infty, \quad v = 0, \quad \frac{\partial u}{\partial y} = 0 \quad (7)$$

$$\frac{1}{\rho_v} \frac{\partial p}{\partial x} = g$$

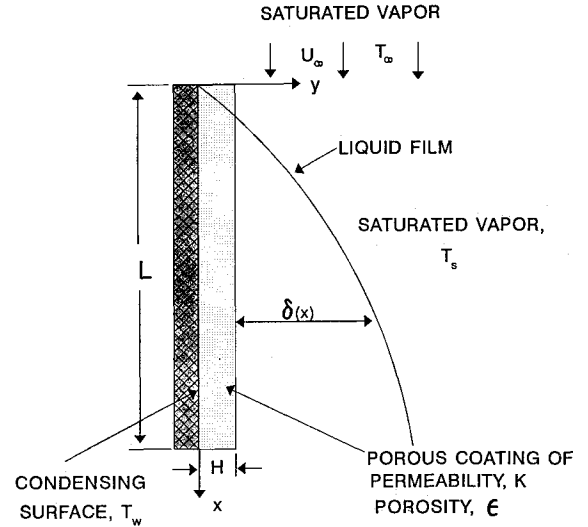


Fig. 1 Schematic of forced convection film condensation within thin porous coatings.

Equation (5) was used for the entire domain, covering the porous and the condensate subregions, by simply correcting the values of  $\nu_e$ ,  $K$ , and  $\varepsilon$ .

The boundary conditions of the present problem are as follows:

$$x = 0: \quad u = U_\infty, \quad v = 0, \quad T = T_\infty \quad (8a)$$

$$y = 0: \quad u = 0, \quad v = 0, \quad T = T_w \quad (8b)$$

$$y = \delta: \quad u_{\delta-} = u_{\delta+} = U_\infty$$

$$\left. \frac{\partial u}{\partial y} \right|_{y=\delta} = 0 \quad (8c)$$

$$T_{\delta-} = T_{\delta+} = T_\infty = T_{\text{sat}}$$

$$q'' = -wh'_{fg}$$

where

$$h'_{fg} = h_{fg}[1 + 0.68c_p(T_\infty - T_w)/h_{fg}] \quad (8d)$$

which accounts for crossflow within the film. In addition to these boundary conditions, matching conditions were satisfied at the porous substrate/pure liquid interface. These conditions included the continuity of longitudinal and transverse velocities, shear stresses, temperatures, and heat fluxes.

Vafai and Thiyagaraja<sup>20</sup> have shown that the Brinkman shear term has to be included in the momentum equation if the interfacing stresses are to match. In the analysis, the effective dynamic viscosity of the porous substrate subregion has been equated to the dynamic viscosity of the liquid in accordance to Refs. 21 and 22. In addition, the effect of the thermal dispersion of the porous coating is assumed constant and has been incorporated into the effective thermal conductivity. Moreover, liquid property variations are reflected by the evaluation at  $T_{\text{ref}} = T_w + (T_\infty - T_w)/3$ , as per the findings of Refs. 23 and 24.

#### Dimensionless Parameters

To simplify the governing equations (mass, momentum, and energy) and the boundary conditions, the following dimensionless variables are introduced:

$$x^* = x/L, \quad y^* = y/L, \quad H^* = H/L \quad (9a)$$

$$u^* = u/U_\infty, \quad v^* = v/U_\infty \quad (9b)$$

$$\theta = (T - T_\infty)/(T_w - T_\infty) \quad (9c)$$

where

$$Re = \rho_f U_\infty L / \mu_f, \quad Pe = U_\infty L / \alpha_f = Re Pr \quad (10)$$

and in the porous substrate subregion

$$Pr_c = \mu_c c_p / k_c, \quad Ra = g\beta(T_w - T_\infty)L^3/\nu\alpha \quad (11a)$$

$$Da = K/L^2, \quad \lambda = FL\varepsilon/\sqrt{K} \quad (11b)$$

where  $Ra$  has taken into account the density difference between the liquid condensate and its vapor.

Upon inserting these nondimensional variables into the governing equations and simplifying, the following transport equations are obtained:

$$\frac{\partial u^*}{\partial x^*} + \frac{\partial v^*}{\partial y^*} = 0 \quad (12)$$

$$u^* \frac{\partial u^*}{\partial x^*} + v^* \frac{\partial u^*}{\partial y^*} = \frac{1}{Re} \frac{\partial^2 u^*}{\partial y^{*2}} - \frac{u^*}{Re Da} - \lambda u^{*2} - \frac{Ra}{Re^2 Pr} \quad (13)$$

$$u^* \frac{\partial \theta}{\partial x^*} + v^* \frac{\partial \theta}{\partial y^*} = \frac{1}{Pe} \frac{\partial^2 \theta}{\partial y^{*2}} \quad (14)$$

These dimensionless equations are valid throughout the porous/fluid composite layer. The dimensionless boundary conditions become

$$x^* = 0: \quad u^* = 1, \quad v^* = 0, \quad \theta = 0 \quad (15a)$$

$$y^* = 0: \quad u^* = 0, \quad v^* = 0, \quad \theta = 1 \quad (15b)$$

$$y^* = \delta^*: \quad u_{\delta^*-}^* = u_{\delta^*+}^* = 1$$

$$\left. \frac{\partial u^*}{\partial y^*} \right|_{y^*=\delta^*} = 0 \quad (15c)$$

$$\theta_{\delta^*-} = \theta_{\delta^*+} = 0$$

$$-(Ja/RePr_c)x^* \left( \frac{\partial \theta}{\partial y^*} \right)_{y^*=0} = \int_0^{\delta^*} u^* dy^*$$

where

$$Ja = (T_\infty - T_w)c_p/h'_{fg} \quad (15d)$$

Calculations were performed to evaluate the effects of the porous coating on the heat transfer rate at the wall. The results for the heat transfer rate are represented in dimensionless form in terms of a local Nusselt number

$$Nu_x = hx/k_f = -x^* k^* \left( \frac{\partial \theta}{\partial y^*} \right)_{y^*=0} \quad (16a)$$

where

$$k^* = k_c/k_f \quad (16b)$$

It should be noted that the conductivity of the fluid was chosen in the formulation of the Nusselt number. This choice resulted in a more meaningful comparison of the heat transfer rate between the porous substrate system and the case where there is no porous coating.

#### Numerical Simulations

Equations (12–15), which describe the entire domain of the problem from the wall to the freestream region, were solved

by a control volume based finite difference method (for details see Carneiro<sup>25</sup>). The calculation domain was divided into a number of control volumes surrounding each grid point. The differential equation was then integrated over each control volume. Piecewise profiles expressing the variation of the dependent variables between grid points were used to evaluate the required integrals. The result was a discretization equation containing the values of the dependent variable(s) for a group of grid points.

The control volume formulation provides that the integral conservation equations of mass, momentum, and energy are satisfied over the control volumes as well as the entire domain. The finite difference equations were subsequently solved using a tridiagonal matrix algorithm (TDMA) which was applied for both the momentum and energy equations. The “Dirichlet” boundary condition was also used in the TDMA.

The numerical scheme used a rectangular grid system which consisted of “NI” horizontal and “I” vertical lines. Since the thickness of the boundary layer  $\delta(x)$  was much smaller than the characteristic length  $L$ , changes in the variables in the streamwise direction were much smaller as compared to changes in the direction perpendicular to the plate. Therefore, a variable grid system was employed whereby there was a finer grid in the  $y^*$  direction and a more coarse grid in the  $x^*$  direction. This expanding grid system gave 1) more accurate results near the wall where the fluid velocity and temperature gradients change dramatically and 2) reduced computational time.

Extensive tests were performed to study the variations of the grid size and the optimal choices of  $\Delta x$  and  $\Delta y$ , while at the same time ensuring stability of the numerical scheme. The grid size was reduced until there was less than 1% difference in the convergent result. A convergence criterion of  $10^{-6}$  was chosen for the film condensation thickness.

In the numerical scheme the space derivatives were approximated by a central difference form, except for the convective terms which used a second upwind difference scheme. A third-order polynomial was assumed to calculate the slope of the temperature profile near the wall<sup>26</sup> which is used in Eq. (16a) to calculate the local Nusselt number.

Comparisons of the heat transfer rate with previous theoretical and numerical results were made to check the validity of the present numerical model. As shown in Figs. 2 and 3, relatively good agreement was found for the following cases of laminar film condensation on a vertical plate with  $H^* = 0$  (no porous coating): 1) pure forced convection and 2) combined body force and forced convection. In these figures, our numerical solutions are compared to the analytical results of Jacobs<sup>27</sup> (pure forced convection) who utilized the Pohlhausen Integral technique and Fujii and Uehara<sup>28</sup> (combined body force and forced convection), who employed an approximate method (Runge-Kutta-Gill method). Both of these solutions

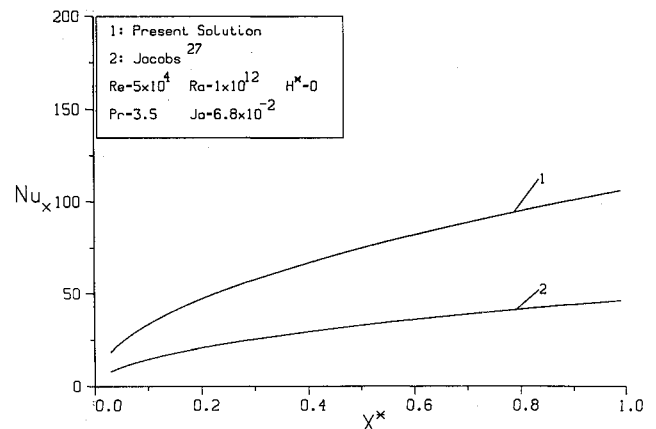


Fig. 2 Comparison of present solution with previous results for the case of no porous coating and Freon-113 as the working fluid.

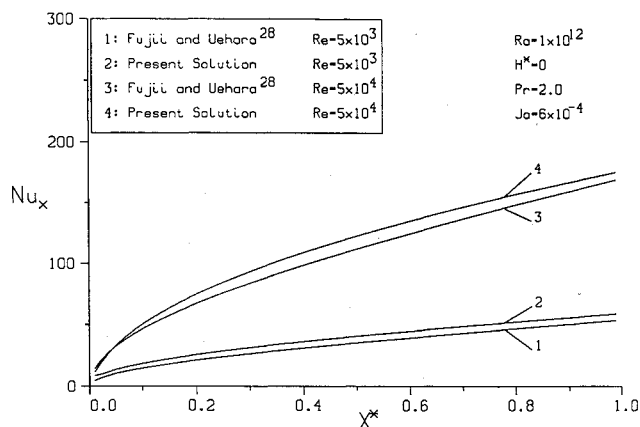


Fig. 3 Comparison of present solution with previous results for the case of no porous coating and water as the working fluid.

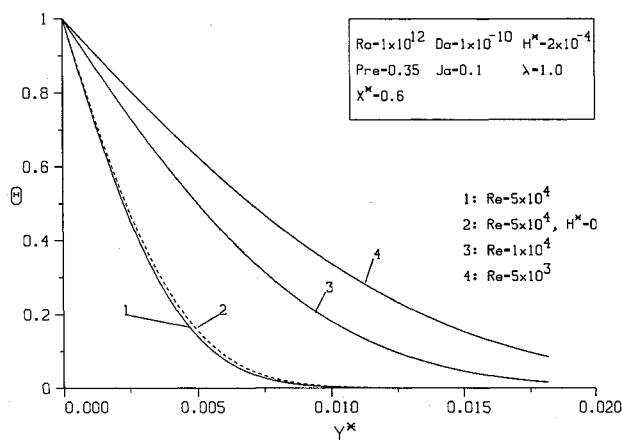


Fig. 4 Temperature distribution within a thin porous coating with variation in the Reynolds number.

neglected the inertia and convection terms which the present numerical solution did not. We have modified the appropriate parameters to account for their fluids, Freon-113<sup>27</sup> and water.<sup>28</sup> It is observed that the heat transfer rate is underpredicted by the approximate methods for the two cases illustrated. In addition to the above forced convection cases, our numerical solutions were also found to be consistent with the classical cases of no porous substrate ( $H^* = 0$ ) and an embedded surface ( $H \rightarrow \infty$ ) when  $Re \rightarrow 0$  (see Carneiro<sup>25</sup>). This first limiting case corresponds to the classical results of laminar film condensation on a vertical surface with no forced convection element. Complete details are found in Ref. 25 and are not repeated here for brevity.

### Results and Discussion

The effects of forced convection on laminar film condensation within thin porous coatings are illustrated in Figs. 4–10. In these figures, water has been used as the working fluid to base property values and variations in the Reynolds number, Rayleigh number, Prandtl number, and Jakob number. Laminar freestream vapor flow has been assumed and porous coating characteristics and experimental conditions from Ref. 19 have been employed.

Figure 4 displays the temperature field for various values of the Reynolds number, for the case where  $Ra$ ,  $Da$ ,  $H^*$ ,  $Pr$ ,  $Ja$ , and  $\lambda$  are fixed, at streamwise location  $x^* = 0.6$ . As expected, the temperature approaches the freestream vapor temperature  $T_\infty$  moving away from the wall and as the Reynolds number increases for a specific transverse location. The influence of the Reynolds number is highlighted even further when in Fig. 4 one compares the slopes of the temperature curves which translate into the heat transfer rates. It is easily seen that the temperature gradient at the wall increases as

the Reynolds number increases due to the larger freestream velocities. Also in Fig. 4, there is a comparison between the case of no porous coating (case 2) and the numerical solution with porous coating for a Reynolds number of  $5 \times 10^4$ . Here, there is better communication and a larger temperature gradient at the wall for the porous substrate case. This is due to the fact that in these numerical solutions, the effective thermal conductivity of the porous coating region is 10 times that of the pure condensate, typical of thin metallic porous substrates.<sup>25</sup>

The effect of the Reynolds number on the heat transfer rate, as represented by the local Nusselt number, is shown in Fig. 5 for fixed values of  $Ra$ ,  $Da$ ,  $H^*$ ,  $Pr$ ,  $Ja$ , and  $\lambda$ . Confirming the results of the temperature profiles, there is an increase in the heat transfer rate as  $Re$  increases. As the freestream vapor velocity increases, the boundary layer thins and there exists sharper temperature gradients at the wall and larger Nusselt numbers. As expected, Fig. 5 shows that the growth rate of  $Nu_x$  decreases with  $x^*$ , or in other words the heat transfer coefficient decreases in the streamwise direction. As shown in this figure, the Nusselt number variations for the case with a porous coating are significantly higher than the case where no porous coating is present ( $H^* = 0$ ). Again, this is because of the relatively high effective thermal conductivity of the porous substrate.

The effect of the Rayleigh number is documented by Fig. 6. This figure can also be used to predict heat transfer rates due to surface subcooling variations and inclination of the porous coated plate. As seen by Eq. (11a), the Rayleigh number is directly related to the surface subcooling and to the gravitational constant, which may be modified by  $\cos \Phi$  where  $\Phi$  would be the angle of inclination away from the vertical. As expected, the computed results predict slightly higher heat transfer coefficients as  $Ra$  increases. Comparing the case of porous coating vs no porous coating, one finds significant heat transfer enhancement as shown in Fig. 6.

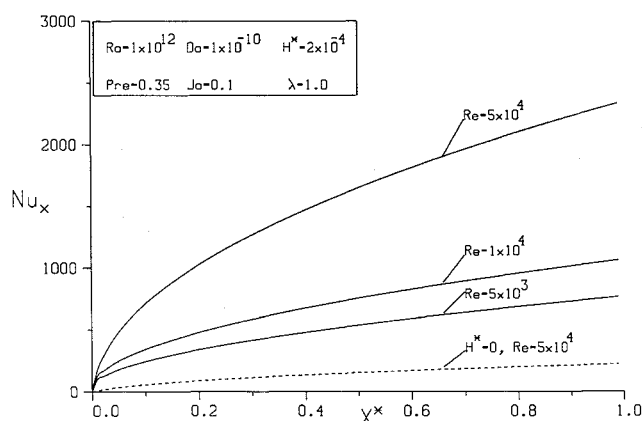


Fig. 5 Effect of Reynolds number on Nusselt number variation.

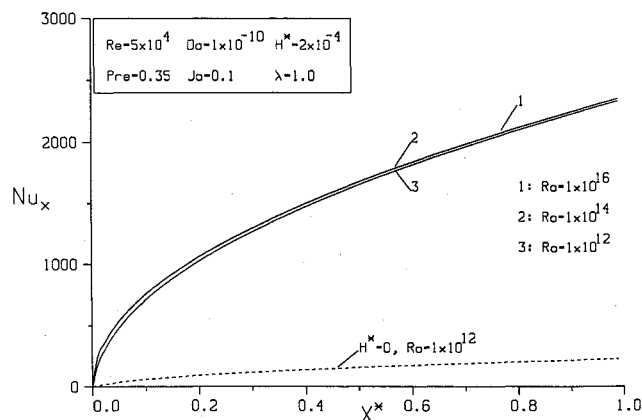


Fig. 6 Effect of Rayleigh number on Nusselt number variation.

It should be noted that the changes in the values of  $Ja$  and of  $\lambda$  on the heat transfer rate were found to be negligible.<sup>25</sup> Minimal changes in  $Nu_x$  were found when  $Ja = 0.01, 0.1$ , and  $1.0$ , or when  $\lambda = 0, 0.5$ , and  $1.0$  for fixed values of  $Re$ ,  $Ra$ ,  $Da$ ,  $H^*$ , and  $Pr_c$ .

Figures 7–10 analyze the most important feature, the effect of the porous coating characteristics on the heat transfer rate during forced convection condensation. The Darcy number which is directly proportional to the permeability of the porous coating has minimal effect on the heat transfer rate for the present problem. In Fig. 7, there are minimal differences when  $Da < 10^{-4}$ . A decrease of  $Da = 10^{-4}$  to  $Da = 10^{-10}$  results in less than a 1% decrease in  $Nu_x$  for the conditions specified. A comparison of the case with a porous coating to

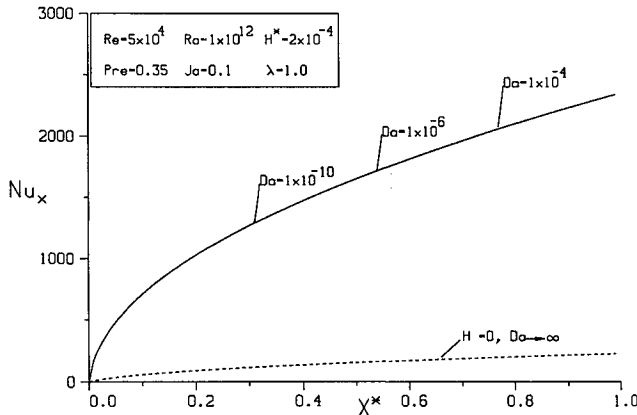


Fig. 7 Effect of Darcy number on Nusselt number variation.

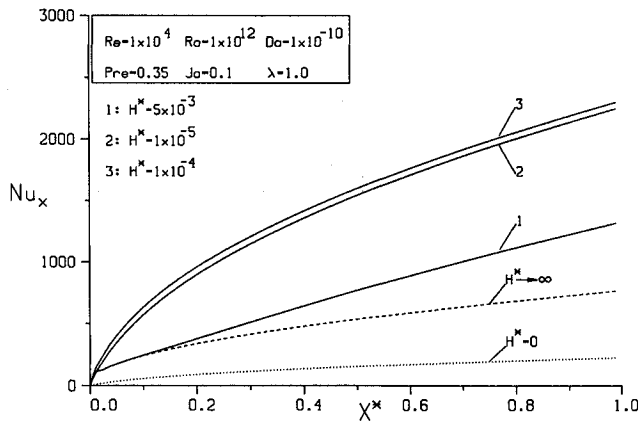


Fig. 8 Effect of porous coating thickness on Nusselt number variation.

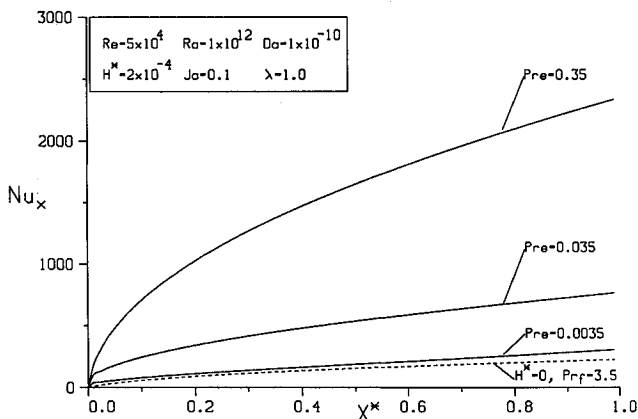


Fig. 9 Effect of effective Prandtl number on Nusselt number variation.

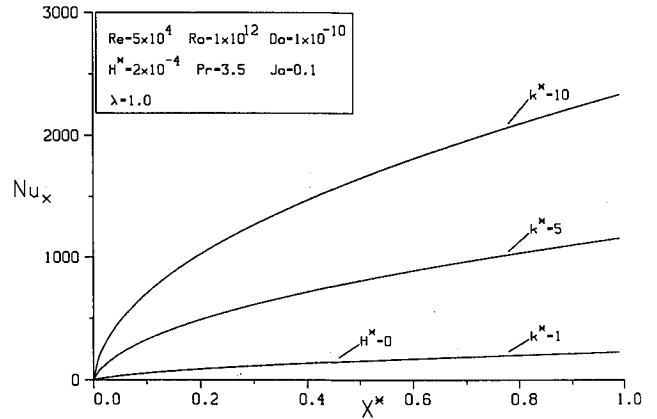


Fig. 10 Effect of effective thermal conductivity on Nusselt number variation.

the case of no porous coating ( $H^* = 0$  and  $Da \rightarrow \infty$ ) is also shown in Fig. 7.

The effect of porous coating thickness is the key parameter in the problem as shown in Fig. 8. It can be seen that the local Nusselt number increases with thickness until an optimal thickness/heat transfer rate is reached. It is hypothesized<sup>25</sup> and shown experimentally<sup>19</sup> that at this optimal thickness the effects of the porous substrate flow resistance and porous/fluid interface condensate displacement began to dominate the effect of the increased thermal conductivity of the porous coating composite. In this figure the  $Nu_x$  increases as  $H^*$  increases from  $1 \times 10^{-5}$  (case 2) to  $1 \times 10^{-4}$  (case 3). As the porous coating further increases (under the prescribed conditions) to  $H^* = 5 \times 10^{-3}$  (case 1), there is a rapid drop-off in the heat transfer rate (simulation of an insulator) and the advancement to the limiting case of an embedded surface ( $H^* \rightarrow \infty$ ). Figure 8 also compares the two limiting cases, where  $H^* \rightarrow \infty$  (embedded surface) and  $H^* = 0$  (plain surface) with the present solutions. It is seen that major enhancements are recognized when a thin porous coating is employed as compared to the plain surface. The case of an impermeable surface embedded in a porous matrix (infinitely thick porous coating) shows heat transfer reduction as compared to the optimal porous coating thickness. It is recognized that the thin porous coating creates continuous movement and intermixing of the condensation from the porous subregion into the fluid subregion due to the flow resistance created by the porous coating subregion. A typical thin porous metallic coating thickness will range from 25 to 250  $\mu\text{m}$ .

The effective Prandtl number effects are shown in Fig. 9 for fixed values of  $Re$ ,  $Ra$ ,  $Da$ ,  $H^*$ ,  $Ja$ , and  $\lambda$ . In this figure the Nusselt number variation for three different values of effective Prandtl number are shown. The values of  $Pr_c$  represent a wide range of fluids such as liquid metals, air, and water. As expected, the Nusselt number increases with an increase in  $Pr_c$ . The case of no porous coating ( $H^* = 0$ ) is represented by the curve  $Pr_c = 3.5$ , which can be compared to the case of  $Pr_c = 0.35$ . In the numerical model, the effective dynamic viscosity of the porous coating subregion is equal to the dynamic viscosity of the pure condensate, while the thermal conductivity ratio between the fluid saturated porous substrate and this pure condensate was equal to 10. As seen by Eq. (11a), Fig. 9 could also be used to predict heat transfer rates based on the value of the effective thermal conductivity of the porous subregion. A better representation is provided by Fig. 10 where  $k^*$  represents the ratio of thermal conductivities of the porous region to that of the pure condensate. The value of  $k^*$  will dictate whether the porous coating will act as a heat transfer enhancer or a retardant under the prescribed conditions. When  $k^*$  is greater than 1.0, there exists heat transfer augmentation, while a value of  $k^*$  less than 1.0 will produce a reduction in the local heat transfer coefficient and, hence,  $Nu_x$ .<sup>25</sup>

### Summary

Laminar forced convection film condensation within thin porous coatings has been investigated by the present work. The dependence of the temperature field and the local Nusselt number on the governing parameters such as the Reynolds number, Rayleigh number, Darcy number, Prandtl number, Jakob number, porous coating thickness, and effective thermal conductivity of the porous substrate were documented. It was found that the freestream vapor flow has a significant effect on the heat transfer rate as compared to pure filmwise condensation, and that there exists major dissimilarities when compared to the case of a plain surface. The use of a porous substrate may enhance the film condensation rate and is dependent on the freestream velocity, the thickness, and the effective thermal conductivity of the porous coating. Under the conditions investigated, the Darcy number and the effect of flow inertia play minimal roles.

### Acknowledgment

Financial support for this research provided by the National Science Foundation through Grant CTS-8909410 is greatly appreciated.

### References

- <sup>1</sup>Nusselt, W., "Die Oberflächenkondensation des Wasser Dampfes," *Zeitschrift des Vereins Deutsches Ingenieure*, Vol. 60, 1916, pp. 541–575.
- <sup>2</sup>Cheng, P., "Film Condensation Along an Inclined Surface in a Porous Medium," *International Journal of Heat and Mass Transfer*, Vol. 24, No. 6, 1981, pp. 983–990.
- <sup>3</sup>Cheng, P., and Chui, D. K., "Transient Film Condensation on a Vertical Surface in a Porous Medium," *International Journal of Heat and Mass Transfer*, Vol. 27, No. 5, 1984, pp. 795–798.
- <sup>4</sup>Udell, K. S., "Heat Transfer in Porous Media Heated from Above with Evaporation, Condensation, and Capillary Effects," *Journal of Heat Transfer*, Vol. 105, Aug. 1983, pp. 485–492.
- <sup>5</sup>Udell, K. S., "Heat Transfer in Porous Media Considering Phase Change and Capillarity—The Heat Pipe Effect," *International Journal of Heat and Mass Transfer*, Vol. 28, No. 2, 1985, pp. 485–495.
- <sup>6</sup>Poulikakos, D., and Orozco, J., "A Study of Condensation on a Vertical Internally Cooled Pipe Embedded in Porous Media," *International Communications in Heat and Mass Transfer*, Vol. 13, No. 2, 1986, pp. 181–192.
- <sup>7</sup>Kaviany, M., "Boundary-Layer Treatment of Film Condensation in the Presence of a Solid Matrix," *International Journal of Heat and Mass Transfer*, Vol. 29, No. 6, 1986, pp. 951–954.
- <sup>8</sup>White, S. M., and Tien, C. L., "Analysis of Laminar Film Condensation in a Porous Medium," *Proceedings of the 1987 ASME-JSME Thermal Engineering Joint Conference* (Honolulu, HI), Vol. 2, March 1987, pp. 401–406.
- <sup>9</sup>White, S. M., and Tien, S. M., "An Experimental Investigation of Film Condensation in Porous Structures," *Proceedings of the 6th International Heat Pipe Conference* (Grenoble, France), 1987, pp. 223–228.
- <sup>10</sup>Plumb, O. A., "Capillary Effects on Film Condensation in Porous Media," AIAA Paper 84-1789, June 1984.
- <sup>11</sup>Shekarriz, A., and Plumb, O. A., "A Theoretical Study of the Enhancement of Filmwise Condensation Using Porous Fins," AIAA/ASME Thermophysics and Heat Transfer Conference (Boston, MA), American Society of Mechanical Engineers Paper 86-HT-31, June 1986.
- <sup>12</sup>Shekarriz, A., and Plumb, O. A., "Enhancement of Film Condensation Using Porous Fins," *Journal of Thermophysics and Heat Transfer*, Vol. 3, No. 3, 1989, pp. 309–314.
- <sup>13</sup>Majumdar, A., and Tien, C. L., "Effects of Surface Tension on Film Condensation in a Porous Medium," *Journal of Heat Transfer*, Vol. 112, Aug. 1990, pp. 751–757.
- <sup>14</sup>Plumb, O. A., Burnett, D. B., and Shekarriz, A., "Film Condensation on a Vertical Flat Plate in a Packed Bed," *Journal of Heat Transfer*, Vol. 112, Feb. 1990, pp. 235–239.
- <sup>15</sup>Chung, J. N., Plumb, O. A., and Lee, W. C., "Condensation in a Porous Region Bounded by a Cold Vertical Surface," *Journal of Heat Transfer*, Vol. 114, Nov. 1992, pp. 1011–1018.
- <sup>16</sup>Renken, K. J., Soltysiewicz, D. J., and Poulikakos, D., "A Study of Laminar Film Condensation on a Vertical Surface with a Porous Coating," *International Communications in Heat and Mass Transfer*, Vol. 16, No. 2, 1989, pp. 181–192.
- <sup>17</sup>Renken, K. J., and Aboye, M., "Analysis of Enhanced Film Condensation Within Inclined Thin Porous-layer Coated Surfaces," *International Journal of Heat and Fluid Flow*, Vol. 14, No. 1, 1993, pp. 48–53.
- <sup>18</sup>Renken, K. J., and Mueller, C. D., "Measurements of Enhanced Film Condensation Utilizing a Porous Metallic Coating," *Journal of Thermophysics and Heat Transfer*, Vol. 7, No. 1, 1993, pp. 148–152.
- <sup>19</sup>Renken, K. J., and Aboye, M., "Experiments on Film Condensation Promotion Within Thin Inclined Porous Coatings," *International Journal of Heat and Mass Transfer*, Vol. 36, No. 5, 1993, pp. 1347–1355.
- <sup>20</sup>Vafai, K., and Thiyagaraja, R., "Analysis of Flow and Heat Transfer at the Interface Region of a Porous Medium," *International Journal of Heat and Mass Transfer*, Vol. 30, No. 7, 1987, pp. 1391–1405.
- <sup>21</sup>Lundgren, T. S., "Slow Flow Through Stationary Random Beds and Suspensions of Spheres," *Journal of Fluid Mechanics*, Vol. 51, Jan. 1972, pp. 273–299.
- <sup>22</sup>Neale, G., and Nader, W., "Practical Significance of Brinkman's Extension of Darcy's Law: Coupled Parallel Flows Within a Channel and a Bounding Porous Medium," *Canadian Journal of Chemical Engineering*, Vol. 52, Aug. 1974, pp. 475–478.
- <sup>23</sup>Poots, G., and Miles, R. G., "Effects of Variable Physical Properties on Laminar Film Condensation of Saturated Steam on a Vertical Flat Plate," *International Journal of Heat and Mass Transfer*, Vol. 10, No. 12, 1967, pp. 1677–1692.
- <sup>24</sup>Lott, R. L., and Parker, J. D., "The Effect of Temperature-Dependent Viscosity on Laminar-Condensation Heat Transfer," *Journal of Heat Transfer*, Vol. 95, May 1973, pp. 267, 268.
- <sup>25</sup>Carneiro, M. J., "The Effect of Forced Convection on Enhanced Film Condensation Within a Porous Substrate," M.S. Thesis, Dept. of Mechanical Engineering, Univ. of Wisconsin–Milwaukee, Milwaukee, WI, 1992.
- <sup>26</sup>Pantankar, S. V., *Numerical Heat Transfer and Fluid Flow*, Hemisphere, New York, 1980.
- <sup>27</sup>Jacobs, H. R., "An Integral Treatment of Combined Body Force and Forced Convection in Laminar Film Condensation," *International Journal of Heat and Mass Transfer*, Vol. 9, No. 7, 1966, pp. 637–648.
- <sup>28</sup>Fujii, T., and Uehara, H., "Laminar Filmwise Condensation on a Vertical Surface," *International Journal of Heat and Mass Transfer*, Vol. 15, No. 2, 1972, pp. 217–233.